JOC The Journal of Organic Chemistry

Article

Elucidation of the E-Amide Preference of N-Acyl Azoles

Yuka Takahashi, Hirotaka Ikeda, Yuki Kanase, Kosho Makino, Hidetsugu Tabata, Tetsuta Oshitari, Satoshi Inagaki, Yuko Otani, Hideaki Natsugari, Hideyo Takahashi, and Tomohiko Ohwada

J. Org. Chem., **Just Accepted Manuscript** • DOI: 10.1021/acs.joc.7b01759 • Publication Date (Web): 02 Oct 2017

ACS Publications

The Journal of Organic Chemistry is published by the American Chemical Society. 1155 Sixteenth Street N.W., Washington, DC 20036

Elucidation of the *E*-Amide Preference of *N*-Acyl Azoles

Yuka Takahashi,[†] Hirotaka Ikeda,[‡] Yuki Kanase,[†] Kosho Makino, [†] Hidetsugu Tabata,[†] Tetsuta Oshitari,[†] Satoshi Inagaki,[‡] Yuko Otani,[‡] Hideaki Natsugari,[†] Hideyo Takahashi,[†,] * Tomohiko Ohwada[‡,] *

[†]Faculty of Pharma Sciences, Teikyo University, 2-11-1 Kaga, Itabashi-ku, Tokyo 173-8605, Japan

[‡]Graduate School of Pharmaceutical Sciences, The University of Tokyo, 7-3-1 Hongo, Bunkyo-ku, Tokyo 113-0033, Japan

Table of Contents Graphic

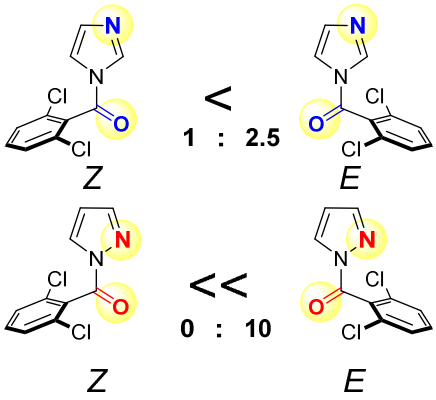

Abstract

The conformational properties of *N*-acyl azoles (imidazole, pyrazole, and triazole) were examined. The *N*-2',4',6'-trichlorobenzoyl azoles were stable in methanol at room temperature, and no hydrolyzed products were observed over 7 days in the presence of 5% trifluoroacetic acid or 5% triethylamine in $CDCl_3$. The high stability may be explained by the double-bond amide character caused by the steric hindrance due to the *ortho*-substituents in the benzoyl group. While specific *E*-amide preferences were observed in *N*-acyl pyrazoles/triazoles, the amides of the imidazoles gave a mixture of *E* and *Z*. One of the conceivable ideas to rationalize this conformational preference may be repulsive interaction between two sets of lone-pair electrons on the pyrazole 2-nitrogen (n_N) and the carbonyl oxygen atoms (n_O) in the *Z*-conformation of *N*-acyl pyrazoles/triazoles. However, analysis of orbital interactions suggested that in the case of the *E*-conformation of *N*-acyl pyrazoles, such electron repulsion is small because of distance. The interbond energy calculations suggested that the *Z*-conformer is involved in strong vicinal σ–σ repulsion along the amide linkage between the σ_{N1N2} and σ_{C1C2} orbitals in the *anti*-periplanar arrangement and between the σ_{N1C5} and σ_{C1C2} orbitals in the *syn*-periplanar arrangement, which lead to the overwhelming *E*-preference in *N*-acyl pyrazoles/triazoles. In the case of *N*-acyl imidazoles, similar vicinal σ–σ repulsions were counterbalanced, leading to a weak preference for the *E*-conformer over the *Z*-conformer. The chemically stable and *E*-preferring *N*-acyl azoles may be utilized as scaffolds in future drug design.

Introduction

In 1962, Staab described *N*-acyl azoles as reactive heterocyclic amides, which have a high degree of reactivity in nucleophilic reactions (e.g., hydrolysis or alcoholysis).[1] Since then, *N*-acyl azoles have been considered to be mild acylating agents as alternatives to acyl halides and anhydrides.[2] Recently, it has been revealed that the sterically hindered *N*-acylimidazoles show better stability toward nucleophiles than unhindered ones, and several stability studies of various *N*-acylimidazoles have been published.[3] In the course of our stereochemical and physicochemical analyses of biologically active molecules,[4] we also found that the 2',6'-disubstituted *N*-benzoyl imidazoles were unexpectedly stable.[5] We presumed that the steric hindrance of 2',6'-disubstituents restricts the benzene ring to being orthogonal to the coplanar structures consisting of the carbonyl group and imidazole, which provides a stable double-bond amide character. These results encouraged us to study the conformations of various *N*-acyl azoles utilizing NMR studies, X-ray crystallography, and calculations. In this report, the conformations of *N*-acyl azoles, especially the *E*-amide preference of the chemically stable *N*-2',4',6'-trisubstituted benzoylated azoles (imidazole, pyrazole, and triazole) are discussed. Furthermore, the elucidation of the origin of the stereoselectivities of amide isomerism by calculation was examined. Our results suggest that the stereospecific, stable conformations found in these azole derivatives should be useful for the next phase of molecular design.

Results and discussion

Amide Conformations of *N*-Acyl Azoles

The simplest *N*-acetyl azoles: Initially, the conformations of *N*-acetyl azoles (*N*-acetyl imidazole **1**,[6a,b] *N*-acetyl pyrazole **2**,[6a,b] *N*-acetyl-1,2,3-triazole **3**,[6a] and *N*-acetyl-1,2,4-triazole

4[6a]) were examined using ^{1}H NMR. Through the examination of the VT NMR spectrum (CD_2Cl_2) of *N*-acetyl imidazole **1**, we found two sets of resonances in a 2:1 ratio at –90 °C, which were assumed to be the *E*/*Z*-amide conformers around the N–(C=O) bond (Figure 1).

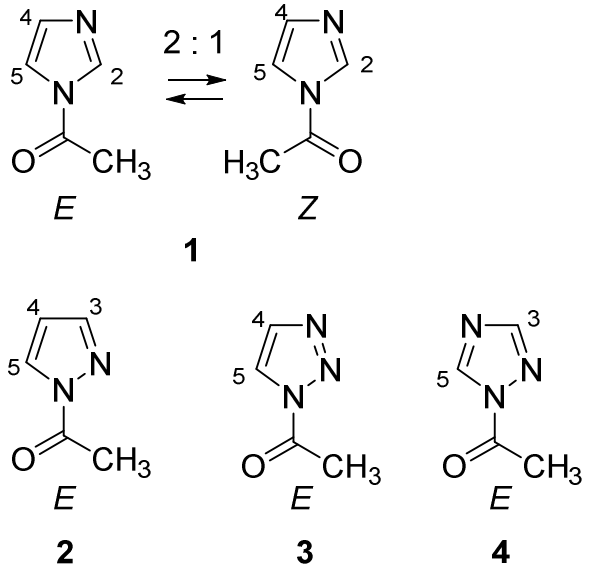

Figure 1. *E*/*Z*-amide conformers of *N*-acetyl azoles.

We assigned the *E*/*Z*-conformations based on the H2-chemical shift. While H2 in the major conformer is observed at δ = 8.04 ppm, H2 in the minor conformer is observed at δ = 8.26 ppm. This downfield shift is caused by a deshielding effect of the carbonyl group in the acetyl moiety, meaning that the minor conformer adopts the *Z*-conformation, and thus the major conformer adopts the *E*-conformation. The activation free energy barrier to rotation of the N—C axis of *E*/*Z*-amide rotamers ($\Delta G^{\ddagger}$)[7] was estimated by VT NMR in two conventional methods, coalescence method and line shape analysis (coalescence method: $\Delta G_c^{\ddagger}$= 9.9 kcal/mol; line shape analysis: $\Delta G^{\ddagger}$ (at -50 °C) = 9.9 kcal/mol)[8] (see the Supporting Information: Figure S1).

Considering this low energy barrier, *N*-acetyl imidazole **1** should exist as *E*/*Z*-conformational mixtures at room temperature. In contrast, for *N*-acetyl pyrazole **2**, *N*-acetyl-1,2,3-triazole **3**, and *N*-acetyl-1,2,4-triazole **4**, only one set of resonances was observed in the VT NMR spectra irrespective of the temperature (–90 °C–100 °C). The fact that H5 is observed at δ = 8.22–8.92 ppm in compounds **2**–**4** caused by a deshielding effect of the carbonyl group in the acetyl moiety confirms that these compounds exist in the *E*-form, as shown in Figure 1. It is true that *N*-acetyl azoles **1**–**4** are less stable so that they are prone to hydrolyzation at ambient temperature. However, it should be noted that **2**–**4** exist in a specific conformation (*E*-isomer) in solvent irrespective of temperature.

***N*-Benzoyl azoles:** We next examined *N*-benzoyl azoles with 2',4',6'-trisubstituents. Following the established method, compounds (**5**–**14**) were synthesized as shown in Scheme 1 (yields and the details of the synthesis are described in experimental).

Scheme 1. Synthesis of *N*-benzoyl azoles.

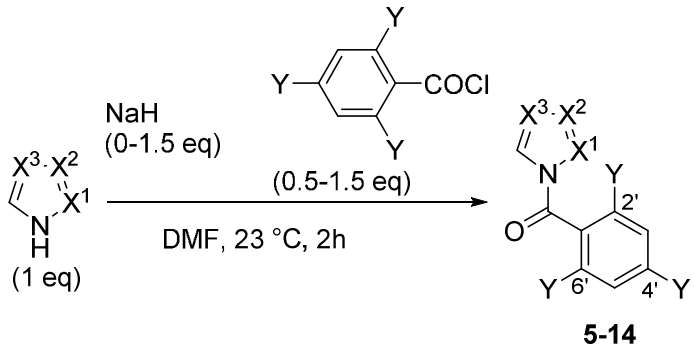

5-14

The conformations determined by VT NMR of *N*-benzoyl azoles (**5**–**8**) (the details are shown in the Supporting Information: Figures S2~S4) are shown in Table 1.

Table 1. *E*/*Z*-amide conformers of *N*-benzoyl azoles.

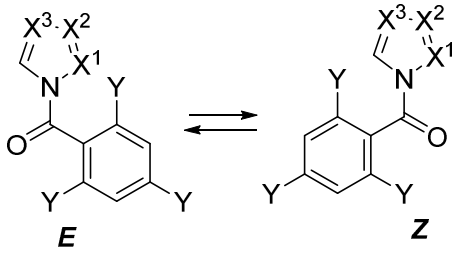

5: X^1 = CH, X^2 = N, X^3 = CH
6: X^1 = N, X^2 = X^3 = CH
7: X^1 = X^2 = N, X^3 = CH
8: X^1 = N, X^2 = CH, X^3 = N

a: Y = H
b: Y = Cl
c: Y = CH_3

	Entry		*E*/*Z*	Tc (°C)	coalescence $\Delta G_c^{\ddagger}$ (kcal/mol)	line shape analysis $\Delta G^{\ddagger}$ (at Tc) (kcal/mol)
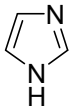	1	**5a**[3]	—	—	—	
	2	**5b**	2.5:1	–50	11.8	12.1
	3	**5c**[3]	2.8:1	–20	13.3	13.3
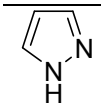	4	**6a**[9]	10:–	—	—	—
	5	**6b**	10:–	—	—	—
	6	**6c**	10:–			
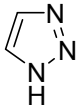	7	**7a**[10]	10:–	—	—	—
	8	**7b**	10:–	—	—	—
	9	**7c**	10:–	—	—	
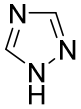	10	**8a**	10:–	—	—	—
	11	**8b**	10:–		—	—

12	**8c**	10:1	–60	10.7	12.0

For *N*-benzoyl imidazole **5a**[3], only one set of resonances was observed in the VT NMR spectrum irrespective of temperature (–90 °C–100 °C).[11] In contrast, *N*-2',4',6'-trichlorobenzoyl imidazole **5b** provided two sets of resonances at –90 °C, which are similar to those of the *E*/*Z*-amide conformers of *N*-acetyl imidazole **1**. Thus, we assigned the *E*/*Z*-conformations based on the H2 shift. Considering the downfield shift of H2 (8.48 ppm) in the minor conformer and the upfield shift of H2 (7.76 ppm) in the major conformer, we determined that the minor conformer adopts the *Z*-conformation,[12] and thus the major conformer adopts the *E*-conformation (*E*/*Z* = 2.5:1). Based on VT NMR, the activation free energy barrier to rotation of the N—C axis of *E*/*Z*-amide conformers of **5b** was estimated (coalescence method: $\Delta G_c^{\ddagger}$= 11.8 kcal/mol; line shape analysis: $\Delta G^{\ddagger}$ (at -50 °C) = 12.1 kcal/mol). Similarly, the two sets[13] of resonances at –90 °C (*E*/*Z* = 2.8:1) were observed in *N*-2',4',6'-trimethylbenzoyl imidazole **5c**[3], and the activation free energy barrier to rotation of the *E*/*Z*-amide conformers was estimated by VT NMR (coalescence method: $\Delta G_c^{\ddagger}$= 13.3 kcal/mol; line shape analysis: $\Delta G^{\ddagger}$ (at -20 °C) = 13.3 kcal/mol).

We next examined the VT NMR spectra of *N*-benzoyl pyrazole **6a**[9], *N*-2',4',6'-trichlorobenzoyl pyrazole **6b**, and *N*-2',4',6'-trimethylbenzoyl pyrazole **6c**. Only one set of resonances for the *E*-amide conformer, which was confirmed by the H5 downfield-shift (δ = 8.40–8.42 ppm), was observed in compounds **6a**, **6b**, and **6c** irrespective of temperature (–90 °C–100 °C). Similarly, in *N*-benzoyl 1,2,3-triazole **7a**[10], *N*-2',4',6'-trichlorobenzoyl 1,2,3-triazole **7b**, and *N*-2',4',6'-trimethylbenzoyl 1,2,3-triazole **7c**, only one set of resonances was observed in the VT NMR spectra irrespective of temperature (–90 °C–100 °C). The downfield shift of H5 (δ = 8.39–8.45 ppm) observed in them confirmed that compounds **7a**–**7c** adopt the specific

conformation (*E*-conformer) irrespective of temperature. Similar results were obtained in the examination of the VT NMR of *N*-benzoyl 1,2,4-triazole **8a**, *N*-2',4',6'-trichlorobenzoyl 1,2,4-triazole **8b**, and *N*-2',4',6'-trimethylbenzoyl 1,2,4-triazole **8c**. Only one set of resonances for the *E*-amide conformer, which was confirmed by the H5 downfield shift, was observed in compounds **8a** and **8b** irrespective of temperature (–90 °C–100 °C). Meanwhile, the minor *Z*-conformer was observed at –90 °C in **8c** (*E*/*Z* = 10:1). The activation free energy barrier to rotation of the N—C axis of the *E*/*Z*-amide conformers of **8c** was estimated by VT NMR (coalescence method: $\Delta G_c^{\ddagger}$= 10.7 kcal/mol; line shape analysis: $\Delta G^{\ddagger}$ (at -60 °C) = 12.0 kcal/mol).

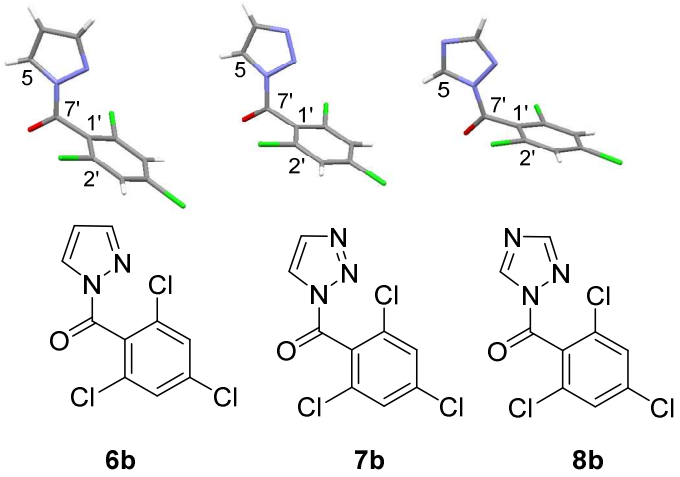

Figure 2 X-ray crystal structures of compounds **6b**, **7b**, and **8b**.

So far, it has been revealed that *N*-acylated (*N*-acetyl, *N*-2',4',6'-trichlorobenzoyl, *N*-2',4',6'-trimethylbenzoyl) imidazoles **1**, **5b**, and **5c** and *N*-2',4',6'-trimethylbenzoyl 1,2,4-triazole **8c** exist in an equilibrium state in solution (*E*/*Z* = 2:1–10:1). On the other hand, other *N*-acyl azoles exclusively adopt the *E*-conformation irrespective of temperature (–90

°C–100 °C) in solution. Fortunately, we succeeded in obtaining **6b**, **7b**, and **8b** as single crystals. Their X-ray analysis supported the stereospecific *E*-conformation (Figure 2) and yielded good information on the conformation of the 2',4',6'-trisubstituted compounds. The dihedral angle (ϕ C5–N–C7'–O) of 172.2–177.6° confirmed the planarity of the amide moiety in compounds **6b**, **7b**, and **8b** (crystal data on **6b**, **7b**, and **8b** are described in the Supporting Information). The dihedral angle (ϕ C2'–C1'–C7'–O) of 79.5–83.5° also confirmed that the benzene ring is nearly orthogonal to the carbonyl group. It is apparent that the substituents at the 2'- and 6'-positions of the benzoyl moiety affect the C7'—C1' axis to form a twisted conformation, and hence the coplanar structures consisting of the carbonyl group and azole ring provide the stable double-bond amide character in *N*-acyl azoles.

In order to examine the stability of the *N*-acylated azoles, we followed the acidic/basic, or nucleophilic cleavage of *N*-2',4',6'-trichlorobenzoyl azoles **5b**, **6b**, **7b**, and **8b** in ^{1}H NMR at room temperature. The acidic/basic stability studies were performed in 5% (v/v) trifluoroacetic acid (TFA) or 5% (v/v) triethylamine (TEA) in $CDCl_3$. All of the compounds were so stable that no hydrolyzed products were observed over 7 days. Similarly, one equivalent amount of diethylamine was treated with the $CDCl_3$ solution of **5b**, **6b**, **7b**, and **8b** for 1 day, and no reaction occurred (the details are described in the Supporting Information: Figures S9–S12). These results confirmed that steric hindrance introduced by the *ortho*-substituents provides the stable double-bond amide character in *N*-benzoyl azoles. These *N*-benzoyl azoles are also stable in methanol.

Effect of 2- and/or 5-substitution of imidazoles on amide equilibrium: We next investigated the conformations of 2- and/or 5-substituted imidazoles (**9b**–**12c**) using VT NMR (Table 2) (the details are shown in the Supporting Information: Figures S5–S8). In 2-methylimidazole

derivatives **9b** and **9c**, two sets of resonances at –90 °C were observed. Based on the upfield shift of H5 (δ = 6.80 ppm for **9b**, δ = 6.70 ppm for **9c**), we determined that the major conformer adopts the *Z*-conformation (*E*/*Z* = 1:20 for **9b**, *E*/*Z* = 1:23 for **9c**). The activation free energy barrier to rotation of the N—C axis of *E*/*Z*-amide rotamers ($\Delta G^{\ddagger}$) was estimated by VT NMR (coalescence method: $\Delta G_c^{\ddagger}$= 11.9 kcal/mol; line shape analysis: $\Delta G^{\ddagger}$ (at -40 °C) = 12.7 kcal/mol for **9b**, coalescence method: $\Delta G_c^{\ddagger}$= 10.3 kcal/mol; line shape analysis: $\Delta G^{\ddagger}$ (at -70 °C) = 10.3 kcal/mol for **9c**). It is important to note that the high selectivity for the *Z*-conformation was observed at –90 °C in **9b** and **9c**, which is in contrast to that of the unsubstituted imidazole derivatives **1**, **5b**, and **5c**. In 5-methyl derivatives **10b** and **10c**, we found one set of resonances for the *E*-conformer irrespective of temperature (–90 °C–100 °C), which was confirmed from the H2 upfield shift (δ = 7.38 ppm for **10b**, δ = 7.38 ppm for **10c**) at –90 °C. These results imply that the conformation, which has the C=O group on the same side of the substituted methyl group, is preferred in **9** and **10**.

Table 2. *E*/*Z*-amide conformers of *N*-benzoyl imidazoles with 2/5 substituents.

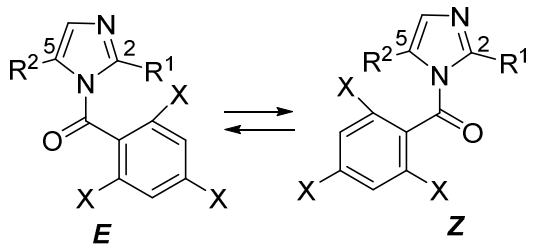

9: $R^1 = CH_3$, $R^2 = H$
10: $R^1 = H$, $R^2 = CH_3$
11: $R^1 = Ph$, $R^2 = H$
12: $R^1 = H$, $R^2 = Ph$

b: X = Cl
c: X = CH_3

Entry		*E*/*Z*	Tc (°C)	coalescence $\Delta G_c^{\ddagger}$ (kcal/mol)	line shape analysis $\Delta G^{\ddagger}$ (at Tc) (kcal/mol)
1	**9b**	1:20	–40	11.9	12.7
2	**9c**	1:23	–70	10.3	10.3
3	**10b**	10:–			
4	**10c**	10:–			
5	**11b**	1:2	–10	13.2	12.6
6	**11c**	–:10			
7	**12b**	4:1	0	14.1	13.1
8	**12c**	10:–			

In a similar manner, the conformations of 2- or 5-phenyl-substituted imidazoles (**11b**–**12c**) were examined by VT NMR. In *N*-2,4,6-trichlorobenzoyl-2-phenyl imidazole **11b**, two sets of resonances at –90 °C were observed. Based on the downfield shift of H5 (δ = 7.81 ppm) in the minor conformer, we determined that the major conformer adopts the *Z*-conformation (*E*/*Z* = 1:2).

The activation free energy barrier to rotation of the N—C axis of the *E*/*Z*-amide rotamers ($\Delta G^{\ddagger}$) was estimated by VT NMR (coalescence method: $\Delta G_c^{\ddagger}$= 13.2 kcal/mol; line shape analysis: $\Delta G^{\ddagger}$ (at -10 °C) = 12.6 kcal/mol). Meanwhile, the corresponding *N*-2,4,6-trimethylbenzoyl derivative **11c** provided only one set of spectra at 22 °C, which was determined to be the *Z*-conformation based on the upfield shift of H5 (δ = 7.06 ppm). Although the separated sharp peaks became broad as the temperature was lowered, no minor conformer was observed at –90 °C in **11c**. Although it is difficult to explain these broad peaks at the lower temperature, the partly reduced rotation of the C2—Ph bond may be responsibe. In *N*-2,4,6-trichlorobenzoyl-5-phenyl imidazole **12b**[14], broad peaks were observed at 22 °C, which became sharp as the temperature decreased. Based on the downfield shift of H2 (δ = 8.42 ppm) in the minor conformer, we determined that the major conformer adopts the *E*-conformation (*E*/*Z* = 4:1) and the activation free energy barrier to rotation of the N—C axis of the *E*/*Z*-amide rotamers ($\Delta G^{\ddagger}$) was estimated by VT NMR (coalescence method: $\Delta G_c^{\ddagger}$= 14.1 kcal/mol; line shape analysis: $\Delta G^{\ddagger}$ (at 0 °C) = 13.1 kcal/mol). In contrast, the corresponding *N*-2,4,6-trimethylbenzoyl derivative **12c**[14] provided only one set of spectra at 22 °C, which was determined to be the *E*-conformation based on the upfield shift of H2 (δ = 7.63 ppm). Similar to **11c**, the separated peaks became broad as the temperature decreased, and no minor conformer was observed at –90 °C in **12c**. Considering these results, it was suggested that the C=O bond preferentially faced in the same direction as the phenyl group in 2- or 5-phenyl-substituted imidazole derivatives (**11** and **12**).

Amide conformation of 3- and 5-disubstituted pyrazoles: We further investigated the conformations of 3- and 5-disubstituted pyrazoles (**13b** and **13c**) using VT NMR (Table 3). In the spectra of *N*-acyl-3,5-dimethylpyrazoles (**13b**, **13c**), only one set of resonances for the *E*-amide conformer, which was confirmed by the 5-CH_3 downfield shift (δ = 2.6-2.7 ppm), was

observed irrespective of temperature (–90 °C–100 °C). Similarly, the corresponding 3,5-diphenylpyrazoles (**14b** and **14c**) provided only one set of resonances presumed to take the *E*-conformation. All these results make it clear that the conformation, which has the C=O group on the same side of the 5- methyl or 5-phenyl group, is exclusively the preferred orientation in **13** and **14**.

Table 3. *E*/*Z*-amide conformers of *N*-benzoyl pyrazoles with 5 substituents.

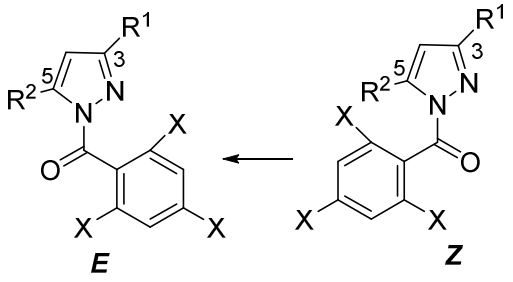

13: $R^1 = R^2 = CH_3$
14: $R^1 = R^2 = Ph$

b: X = Cl
c: $X = CH_3$

Entry		*E*/*Z*
1	**13b**	10:–
2	**13c**	10:–
3	**14b**	10:–
4	**14c**	10:–

Since imidazole derivatives **9b** and **11b** and pyrazole derivatives **13b** and **14b** were obtained as single crystals, we performed their X-ray structure analysis (crystal data on **9b**, **11b**, **13b**, and **14b** are described in the Supporting Information). As shown in Figure 3, the conformations of **9b**, **13b**, and **14b** were consistent with the results observed in the NMR spectra. However,

N-2,4,6-trichlorobenzoyl-2-phenyl imidazole **11b** exhibited the *E*-conformation, which is the minor orientation in solution. The presence of the *E*-conformation in the crystal could be a fortuitous crystal packing arrangement effected by π–π-stacking of two phenyl groups.

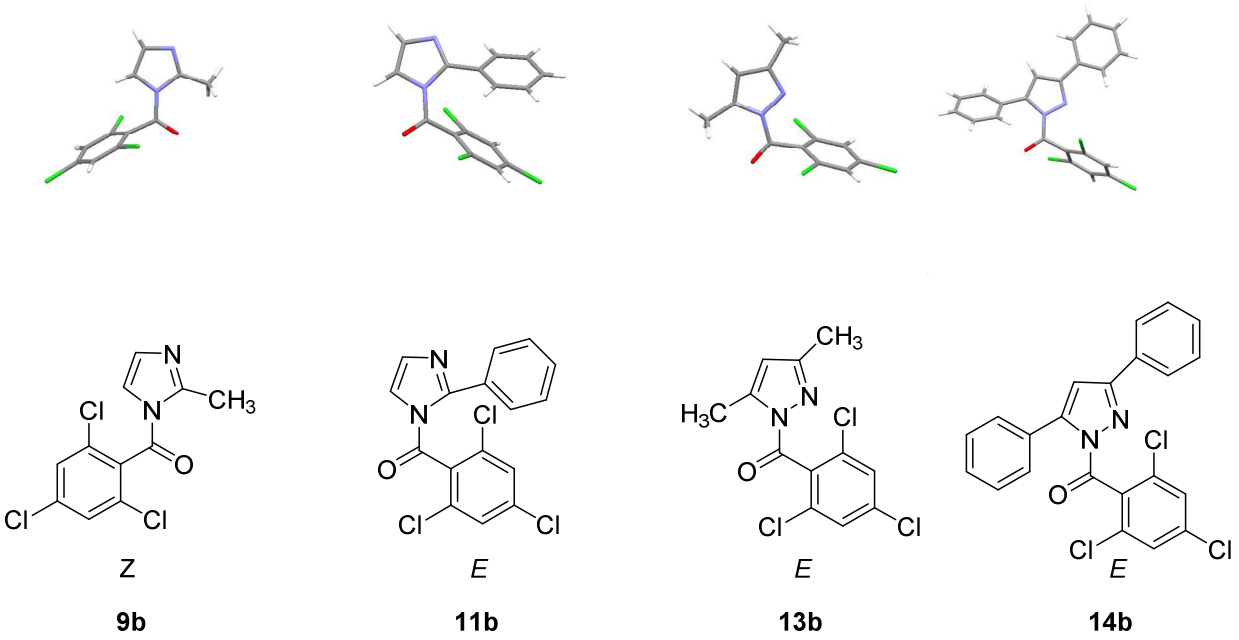

Figure 3. X-ray crystal structures of compounds 9b, 11b, 13b, and 14b.

Computational study of the relative stability of *E*/*Z*-amide conformations

DFT calculations were carried out to evaluate the relative stability of the *E*- and *Z*-amide conformations of the experimentally studied molecules and simplified molecules. The relative energy differences of two conformers were estimated on the basis of geometries fully optimized with B3LYP/6-311++G(d,p) with energy calculations with B3LYP/6-311++G(d,p) on the SCRF/IEFPCM model in CH_2Cl_2. Zero point energy (ZPE) correction was made on the basis of the frequency calculation with B3LYP/6-311++G(d,p). We found that in the cases of *N*-2,4,6-trimethylbenzoyl-substituted amides (**6c**, **7c**, and **8c**), the dispersion effects between

methyl groups and the other fragments were affected by the solvation model (i.e., overestimation), and the energy difference between E and Z conformations were seriously underestimated. Therefore, in order to estimate the dispersion effects accurately in the solvent model, we used the energy difference based on the SCRF/IEFPCM model in CH_2Cl_2 in M06-2X/6-311G(d,p) with the M06-2X/6-311G(d,p) fully optimized structures. Zero point energy (ZPE) correction was also made on the basis of the frequency calculation with M06-2X/6-311G(d,p). The similar methods were also applied to the related imidazole (**5c**), *N*-2,4,6-trichorobenzoyl-substituted amides (**5b**, **6b**, **7b**, and **8b**) and *N*-benzoyl-substituted amides (**5a**, **6a**, **7a**, and **8a**) for comparison. The trends and magnitudes of the relative energies based on B3LYP/6-311++G(d,p) and M06-2X/6-311G(d,p) were comparable in the cases of *N*-2,4,6-trichorobenzoyl-substituted amides (**5b**, **6b**, **7b**, and **8b**) and *N*-benzoyl-substituted amides (**5a**, **6a**, **7a**, and **8a**). The relative energy differences were represented in terms of difference in Gibbs free energy estimated after correction of vibration energies at 300 K (27 °C). All the values are compiled in Tables 4–7. All the optimized structures are shown in Supporting Information. We cited the M06-2X/6-311G(d,p) solvent model energies, if they were available, and otherwise the B3LYP/6-311++G(d,p) solvent model energies were cited in the text.

Table 4. Calculated Energy Difference (in kcal/mol) of Amide Isomers of Imidazole Derivatives [a]

compound	B3LYP/ 6-31G(d) optimization ΔΔH(*Z*-*E*)	B3LYP/ 6-311++G(d,p) optimization ΔΔH(*Z*–*E*)	IEFPCM-B3LYP/ 6-311++G(d,p) single point (CH_2Cl_2)	**ΔΔG (*Z*-*E*) (at 300K)**	Experimental Ratio of *E*/*Z* [c] *E* : *Z*
1 (*N*-acetyl)	+0.19	+0.30	+0.18	+0.21	2 : 1
5a	+0.39	+0.47	+0.35 [+0.22] [b]	+0.32 [+0.22] [b]	ND
5b	+0.32	+0.46	+0.37 [+0.23] [b]	+0.34 [+0.18] [b]	2.5 : 1
5c	+0.32	+0.46	+0.40 [+0.38] [b]	+0.44 [+0.67] [b]	2.8 : 1
9b	-2.18	-1.79	-1.77	-1.32	1 : 20
9c	-2.18	-2.18	-1.93	-2.69	1 : 23
10b	+2.32	+2.22	+1.94	+3.70	10 : -
10c	+2.47	+2.47	+2.01	+2.46	10 : -
11b	-1.16	-0.58	-1.16	-2.17	1 : 2
11c	-1.30	-1.26	-1.55	-3.19	- : 10
12b	+1.22	+0.85	+1.44	+2.10	4 : 1
12c	+1.50	+1.64	+1.84	+3.91	10 : -
***N*-formyl**	+0.41	+0.56	+0.53	+0.48	ND
***N*-acetyl-2-Me**	-2.38	-2.22	-1.91	-1.97	ND
***N*-acetyl-5-Me**	+2.42	+2.42	+1.79	+1.80	ND
***N*-acetyl-2,5-diMe**	-0.14	-0.08	-0.29	-0.18	ND

a) The energy difference (*Z* form – *E* form) was shown. Positive values showed *E* form is more stable, and negative values showed *Z* form is more stable.
b) Due to adequate evaluation of dispersion effect, the value was obtained by the single point calculation with energy estimation with M06-2X/6-311G(d, p) on the basis of the optimized structure with M06-2X/6-311G(d, p).
c) The ratios of *E*/*Z* conformations observed experimentally (600 MHz, CD_2Cl_2, at -90 °C). ND=not determined.

Table 5. Calculated Energy Difference (in kcal/mol) of Amide Isomers of Pyrazole Derivatives [a]

compound	B3LYP/ 6-31G(d) optimization ΔΔH(Z-*E*)	B3LYP/ 6-311++G(d,p) optimization ΔΔH(*Z*–*E*)	IEFPCM-B3LYP/ 6-311++G(d,p) single point (CH_2Cl_2)	**ΔΔG (*Z*-*E*) (at 300K)**	Experimental Ratio of *E*/*Z* [c] *E* : *Z*
2 (*N*-acetyl)	+6.45	+6.35	+2.99	+3.05	10 : -
6a	+5.12	+4.55	+1.77 [+1.66] [b]	+1.85 [+2.10] [b]	10 : -
6b	+4.76	+4.55	+2.34 [+2.30] [b]	+2.30 [+2.38] [b]	10 : -
6c	+2.17	+3.24	+1.36 [+1.52] [b]	[+1.49] [b]	10 : -
5-me Cl	+7.98	+7.51	+4.93	+6.71	ND
5-me Me	+6.54	+6.02	+3.80	+4.13	ND
13b	+6.89	+7.48	+4.91	+6.90	10 : -
13c	+6.54	+5.97	+3.73	+3.97	10 : -
5-ph Cl	+6.65	+6.04	+4.30	+4.98	ND
5-ph Me	+5.03	+4.81	+3.56	+4.79	ND
14b	+6.35	+5.73	+3.66	+4.10	10 : -
14c	+5.03	+4.84	+3.62	+4.97	10 : -

a) The energy difference (*Z* form – *E* form) was shown. Positive values showed E form is more stable, and negative values showed *Z* form is more stable.
b) Due to adequate evaluation of dispersion effect, the value was obtained by the single point calculation with energy estimation with M06-2X/6-311G(d, p) on the basis of the optimized structure with M06-2X/6-311G(d, p).
c) The ratios of *E*/*Z* conformations observed experimentally (600 MHz, CD_2Cl_2, at -90 °C). ND=not determined.

Table 6. Calculated Energy Difference (in kcal/mol) of Amide Isomers of 1,2,3-Triazole Derivatives [a)]

compound	B3LYP/ 6-31G(d) optimization ΔΔH(*Z*-*E*)	B3LYP/ 6-311++G(d,p) optimization ΔΔH(*Z*–*E*)	IEFPCM-B3LYP/ 6-311++G(d,p) single point (CH_2Cl_2)	**ΔΔG (*E*-*Z*) (at 300K)**	Experimental Ratio of *E*/*Z* [c] *E* : *Z*
3 (*N*-acetyl)	+6.38	+6.51	+3.03	+3.08	10 : -
7a	+5.10	+4.75	+1.84 [+1.81] [b]	+1.83 [+1.83] [b]	10 : -
7b	+4.61	+4.63	+2.43 [+2.14] [b]	+2.33 [+1.77] [b]	10 : -
7c	+3.79	+3.50	+1.54 [+1.52] [b]	[+1.49] [b]	10 : -

a) The energy difference (*Z* form – *E* form) was shown. Positive values showed *E* form is more stable, and negative values showed *Z* form is more stable.
b) Due to adequate evaluation of dispersion effect, the value was obtained by the single point calculation with energy estimation with M06-2X/6-311G(d, p) on the basis of the optimized structure with M06-2X/6-311G(d, p).
c) The ratios of *E*/*Z* conformations observed experimentally (600 MHz, CD_2Cl_2, at -90 °C)

Table 7. Calculated Energy Difference (in kcal/mol) of Amide Isomers of 1,2,4-Triazole Derivatives [a)]

compound	B3LYP/ 6-31G(d) optimization ΔΔH(*Z*-*E*)	B3LYP/ 6-311++G(d,p) optimization ΔΔH(*Z*–*E*)	IEFPCM-B3LYP/ 6-311++G(d,p) single point (CH_2Cl_2)	**ΔΔG (*E*-*Z*) (at 300K)**	Experimental Ratio of *E*/*Z* [c] *E* : *Z*
4 (*N*-acetyl)	+5.75	+5.64	+2.56	+2.53	10 : -
8a	+4.46	+3.86	+1.30 [+1.72] [b]	+1.45 [+2.02] [b]	10 : -
8b	+3.97	+3.73	+1.79 [+1.76] [b]	+1.71 [+1.62] [b]	10 : -
8c	+3.05	+2.57	+0.92 [+0.85] [b]	[+1.18] [b]	10 : 1

a) The energy difference (*Z* form – *E* form) was shown. Positive values showed *E* form is more stable, and negative values showed *Z* form is more stable.
b) Due to adequate evaluation of dispersion effect, the value was obtained by the single point calculation with energy estimation with M06-2X/6-311G(d, p) on the basis of the optimized structure with M06-2X/6-311G(d, p).
c) The ratios of *E*/*Z* conformations observed experimentally (600 MHz, CD_2Cl_2, at -90 °C)

Energetics of *N*-Aroyl Derivatives

Imidazoles (Table 4): The optimized structures of *N*-substituted benzoyl imidazoles **5b** and **5c** take bisected structures in which the aromatic ring is perpendicular with respect to the amide plane, consistent with the X-ray structures (Figure 3: **9b**, **11b**). Therefore, the benzene moiety is unconjugated with the amide, indicating that the benzene π system has little effect on the bias of amide *E*–*Z*-conformations in the ground state. The calculated energy differences of the amide *E*/*Z*-conformers of **5b** (*E*-isomer, favored by 0.18 kcal/mol (ΔΔG (*E*-*Z*) (at 300K)) and **5c** (*E*-isomer, favored by 0.67 kcal/mol) are consistent with the observed ratios of the isomers (*E*:*Z* = 2–3:1) in ^{1}H NMR spectroscopy (Table 1).

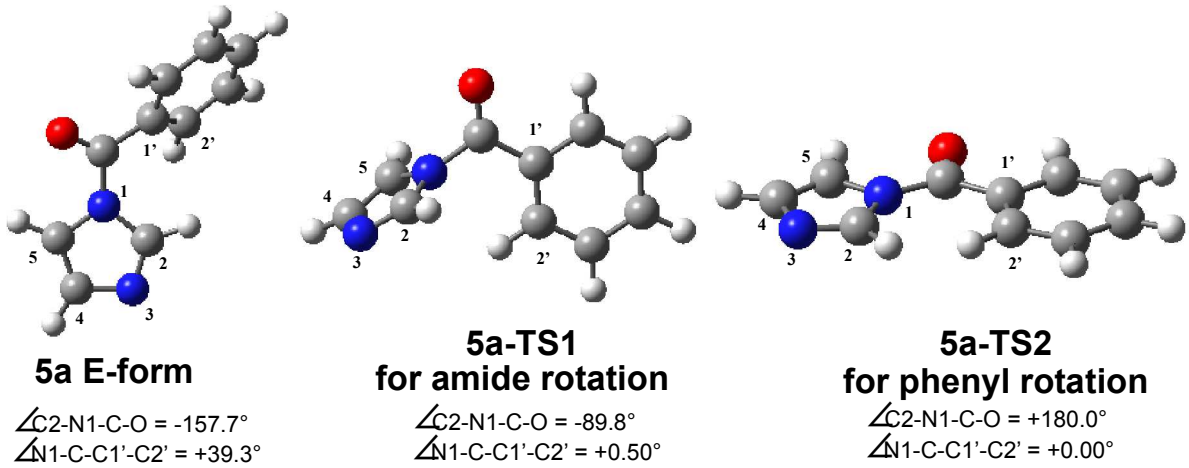

Figure 4. DFT optimized structures of compound 5a E-form and transition state structures for amide rotation (5a-TS1) and for phenyl rotation (5a-TS2).

In the case of *N*-benzoyl imidazole **5a**, although giving a single set of signals in the ^{1}H NMR experiment, the calculated energy difference of the *E*/*Z* amide conformers of **5a** (*E*-isomer, favored by 0.22 kcal/mol) was of similar magnitude to those of **5b** and **5c**. Thus, we calculated

the activation energies for the rotation of amide rotation (**5a-TS1**) and that for the phenyl group (**5a-TS2**) (Figure 4) and found that the activation energies for the rotation of the phenyl group (5.56 kcal/mol; PCM model in CH_2Cl_2) is comparable in magnitude to that for amide rotation (5.83 kcal/mol; PCM model in CH_2Cl_2). Furthermore, the rotational barrier of the latter amide is much smaller than those of the conventional amides (15–20 kcal/mol). Therefore, we cannot distinguish the amide *E*- and *Z*-conformations of **5a** on the NMR time scale, which will lead to an unresolved single set of signals in the NMR experiments.

On the other hand, the calculated activation energies for the amide *E*–*Z* rotation of *N*-2',4',6'-trisubstituted benzoyl imidazoles **5b** and **5c** are 16.80 kcal/mol from the *E*-isomer of **5b** and 11.80 kcal/mol from the *E*-isomer of **5c**, respectively. These values of **5b** and **5c** are much larger than that of *N*-unsubsituted benzoyl derivative **5a** (5.83 kcal/mol). The magnitude of these values matches the experimentally observed values of 12.1 kcal/mol for **5b** (at –50 °C) and 13.0 kcal/mol for **5c** (at –20 °C).

Experimentally, we found that the substitution of a methyl group at the 2-position of *N*-aroyl imidazoles (**9b** and **9c**) distinctly switched the conformational preference to the *Z*-conformation, whereas the 2-unsubstituted prototypes (**5b** and **5c**) showed a weak preference for the *E*-form (Tables 1, 2). The calculated energy difference of the *Z*- and *E*-conformers of 2-methyl derivatives (**9b** and **9c**) was 1.32 and 2.69 kcal/mol, respectively, which is consistent with a strong preference for the *Z*-conformation. Other experimental substitution effects were consistent with the calculations (see the Supporting Information).

Pyrazoles (Table 5): *N*-Aroyl-pyrazoles **6a**, **6b**, and **6c** favored *E*-conformations (Table 1). Calculations showed that the energy differences between the *E*- and *Z*-conformations are 2.10,

2.38, and 1.49 kcal/mol, respectively, which is consistent with the overwhelming experimental bias. When methyl (**13b** and **13c**) or phenyl (**14b** and **14c**) substituents were introduced at the 3- and 5-positions of pyrazoles, a strongly biased preference for the *E*-conformation was found (Table 3). This is consistent with the increase in the calculated energy differences of 6.90 kcal/mol (**13b**), 3.97 kcal/mol (**13c**), 4.10 kcal/mol (**14b**), and 4.97 kcal/mol (**14c**), respectively. The substituent at the 3-position is distal, and it is expected that the 3-substituent will have little influence on the conformational preference. The calculated energy difference (6.71 kcal/mol) of the *E*/*Z*-conformers of the 5-monomethyl-substituted derivative is similar in magnitude to that of the 3,5-dimethyl **13b (**6.90 kcal/mol). A similar situation is found in the case of phenyl substitution: energy differences of the *E*/*Z*-amide conformers of the corresponding 5-monophenyl-subsitututed pyrazole derivatives were 4.98 kcal/mol (*N*-trichlorobenzoyl-5-Ph-prazole derivative) and 4.79 kcal/mol (*N*-trimethylbenzoyl-5-phenyl-prazole derivative), respectively, which are very similar in magnitude to those of 3,5-diphenyl-prazole derivatives, i.e., 4.10 kcal/mol for **14b** and 4.97 kcal/mol for **14c**. An overwhelming preference for the *E*-conformation is consistent among the series of compounds comprising 3,5-unsubstituted (**6a**–**6c**, Table 1), virtual 5-substituted, and 3,5-disubstituted derivatives (**13b**, **13c**, **14b**, and **14c**), even though a steric demand introduced by substitution at the 5-position of pyrazole is present. Therefore, the conformational preference can again be derived from nonsteric factors, and probably the determining factor is the unfavorable interaction between the 2-nitrogen atom and the N–(C=O) groups intrinsic in the *Z*-conformation.

1,2,3-Triazoles (Table 6): *N*-Aroyl-1,2,3-triazoles **7a**, **7b**, and **7c** favored *E*-conformations (Table 1). Calculations showed that the energy differences between the *E*- and *Z*-conformations are 1.83, 1.77, and 1.49 kcal/mol respectively, which is consistent with the overwhelming experimental *E*-bias.

1,2,4-Triazoles (Table 7): In a manner similar to *N*-aroyl-1,2,3-triazoles, calculations showed that the energy differences between the *E* and *Z* conformations of *N*-aroyl-1,2,4-triazoles (**8a**, **8b**, and **8c**) are 2.02, 1.62 and 1.18 kcal/mol, respectively, which is consistent with the experimental *E* bias (Table 1). In the case of **8c**, the equilibrating *Z*-form can be observed due to the intermediate magnitude of the energy difference.

Energetics of *N*-Acetyl Derivatives

While simple *N*-acetyl derivatives of imidazole (**1**) gave a slightly biased mixture of *E*- and *Z*-isomers (*E*:*Z* = 2:1) (see the Supporting Information: Figure S1), *N*-acetyl derivatives of pyrazole (**2**), 1,2,3-triazole (**3**), and 1,2,4-triazole (**4**) gave a single conformation (*E*-conformation) (Figure 1). The magnitude of the calculated energy differences of the *E*- and *Z*-conformers is reasonably consistent with this experimental trend: **1**, 0.21 kcal/mol; **2**, 3.05 kcal/mol; **3**, 3.08 kcal/mol; and **4**, 2.53 kcal/mol favoring the *E*-conformation. In both the experimental and theoretical results, the conformational preferences of *N*-acetyl derivatives (Figure 1) completely coincided with those of *N*-aroyl derivatives (Table 1). In the cases of pyrazole (**2**), 1,2,3-triazole (**3**), and 1,2,4-triazole (**4**), the *N*-acetyl group can induce complete bias of *E*–*Z* isomerization. This result supported the hypothesis that conformational preferences can be derived from nonsteric factors, probably due to the presence of the 2-nitrogen atom in the heterocyclic molecules.

Origin of the stereoselectivities of amide isomerism

We focused on analysis of *N*-acetyl pyrazole **2** and *N*-2',4',6'-trichlorobenzoyl pyrazole **6b** to determine the origin of the *E*-conformer preference. The electronic structures of the molecules were analyzed using bond model analysis,[15] which is able to evaluate the bond orbital interactions in molecules.[16]

Analysis of Orbital Interactions

Vicinal σ–σ electron repulsion

Pyrazole (Table 8): The interactions to be considered are the repulsive interactions between the σ orbitals (σ electrons), vicinal around the C–N amide linkage, connecting the pyrazole nitrogen atom and the acetyl carbonyl carbon atom of the *N*-acetyl pyrazole **2** since the magnitude of the interactions is reasonably affected by the rotation around the C–N amide bond. The calculated interbond energies (IBEs) are listed in Table 8. The IBEs showed that the repulsions between the σ orbitals, vicinal with respect to the amide linkage, differed greatly in energy between the *E*- and *Z*-conformers of **2**. The repulsion of the C1–C2 σ orbital of the acetyl group against the N1–N2 σ orbital of the pyrazole ring is surprisingly strong in the *Z*-conformer (+0.198 au [hartree]) in comparison with that of the C1–C2 σ orbital against the N1–N2 σ orbital in the *E*-conformer (+0.062 au) (Figure 5). It is worth noting that in the *Z*-conformer, the N1–N2 and C1–C2 bonds are in the *anti*-periplanar configuration and the corresponding bonds (i.e., N1–N2 and C1–C2 bonds) in the *E*-conformer are in the *syn*-periplanar configuration. On the other hand, the repulsion of the carbonyl C1–C2 σ bond against the pyrazole N1–C5 σ bond in the *Z*-conformer is greater (+0.193 au) than that of the carbonyl C1–C2 σ bond against the N1–C5 σ bond in the *E*-conformer (+0.072 au). The σ orbitals in the *Z*-conformation are in the *syn*-periplanar configuration, and the σ orbitals in the *E*-conformation are in the *anti*-periplanar configuration, respectively (see Figure 5).

Furthermore, a similar *anti*-periplanar vicinal electron repulsion between σ–σ orbitals is also found in the combination of the pyrazole N1–N2 σ bond against the carbonyl C1–O σ bonds in

Table 8 IBEs (au,hartree) of bond orbitals in *N*-acetyl pyrazole **2**[a]

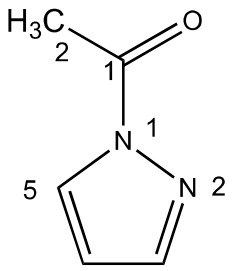

2 Z isomer

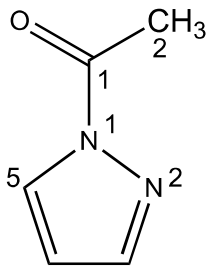

2 E isomer

Repulsion between σ–σ orbitals	Z isomer	E isomer	Δ
$\sigma_{NN} \longleftrightarrow \sigma_{C1C2}$	**0.198**	**0.062**	-0.136
$\sigma_{N1C5} \longleftrightarrow \sigma_{C1C2}$	**0.193**	**0.072**	-0.121
$\sigma_{NN} \longleftrightarrow \sigma_{C1O}$	**0.005**	**0.118**	0.113
$\sigma_{N1C5} \longleftrightarrow \sigma_{C1O}$	**0.082**	0.031	-0.051
	Z isomer	E isomer	Δ
Delocalization between σ–σ* orbitals			
$\sigma_{NN} \longrightarrow \sigma^*_{C1C2}$	-0.005	0.020	0.025
$\sigma_{C1C2} \longrightarrow \sigma^*_{NN}$	-0.149	-0.004	0.145
$\sigma_{N1C5} \longrightarrow \sigma^*_{C1C2}$	0.066	-0.028	-0.094
$\sigma_{C1C2} \longrightarrow \sigma^*_{N1C5}$	-0.001	-0.128	-0.127
$\sigma_{NN} \longrightarrow \sigma^*_{C1O}$	0.000	0.005	0.005
$\sigma_{C1O} \longrightarrow \sigma^*_{NN}$	0.009	-0.087	-0.096
$\sigma_{N1C5} \longrightarrow \sigma^*_{CO}$	-0.011	0.003	0.014
$\sigma_{CO} \longrightarrow \sigma^*_{N1C5}$	-0.101	0.005	0.106

a) au. =627.51 kcal/mol

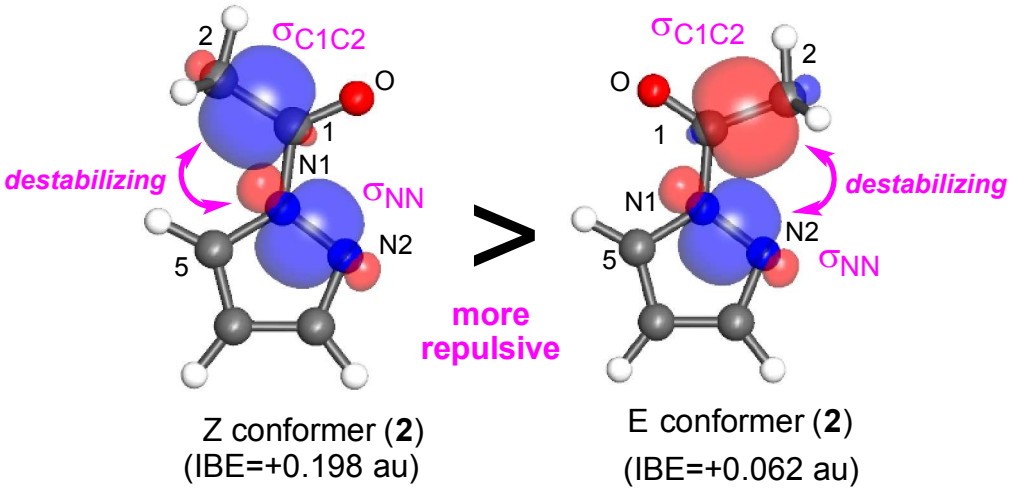

Figure 5. Isosurfaces of the σ_{NN} and σ_{CC} orbitals of *N*-acetyl pyrazole **2**.

Isovalue 0.067 was used.

the *E*-conformation (+0.118 au), which was slightly larger than the *anti*-periplanar vicinal repulsion of the pyrazole N1–C5 σ bond against the carbonyl C1–O σ bonds in the *Z*-conformation (+0.082 au). These repulsion interactions arising from the carbonyl C1–O σ bonds almost compensate for each other in the *E*- and *Z*-conformations. Therefore, strong repulsions of the carbonyl C–C2 σ bond against the pyrazole N1–N2 and N1–C5 bonds in the Z-conformer are detected and these are likely the predominant factors in destabilizing the Z-conformer, leading to biased preference for the *E*-conformer.

N-2',4',6'-Trichlorobenzoyl pyrazole: The electronic structure of *N*-2',4',6'-trichlorobenzoyl pyrazole **6b** was also analyzed. The σ_{N1N2} and σ_{C1C2} orbitals of **6b** are shown in Figure 6 together with the values of IBEs. The calculated IBEs are shown in Supporting Table S1. The IBEs indicate strong repulsion between the σ_{N1N2} and σ_{C1C2} orbitals in the *anti*-periplanar arrangement (*Z*-conformer). In a manner similar to **2**, a strong repulsion of the carbonyl C1–C2 σ bond

against the pyrazole N1–C5 bonds in the *syn*-periplanar arrangement (*Z*-conformer) was found, contributing to destabilization of the *syn*-periplanar interaction in the *Z*-conformer. Therefore, the stability of the *Z*-conformer of **6b** is also controlled by the repulsion of the σ orbitals.

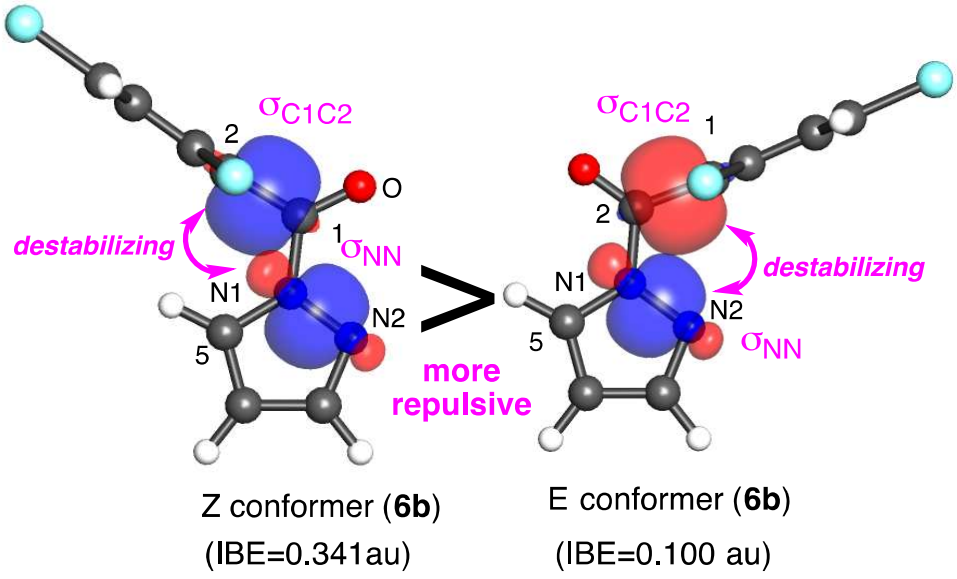

Figure 6. Isosurfaces of the σ_{NN} and σ_{CC} orbitals of *N*-2', 4', 6'-trichlorobenzoyl pyrazole **6b**. Isovalue 0.067 was used.

n–n Electron Repulsion One of the conceivable ideas to rationalize the conformational preference may be repulsive interaction between two sets of lone-pair (nonbonding) electrons on the pyrazole 2-nitrogen (n_N) and the carbonyl oxygen atoms (n_O) in the *Z*-conformation of *N*-acetyl pyrazole **2** (Figure 7(a)). The repulsion energy of n_O–n_N in the *Z*-conformation of **2** is +0.016 au (hartree), according to the IBE. In the case of the *E*-conformation of **2**, the electron repulsion between the 2-nitrogen lone-pair electrons (n_N) and the carbonyl oxygen lone-pair electrons (n_O) is negligible; therefore the energy difference in the repulsive interaction of n_O–n_N between the *Z*- and *E*-conformations is much smaller than that of the above-mentioned σ–σ

electron repulsion (vide infra). This is because these two nonbonding orbitals are distal, and the interaction is insignificant.

n–σ* Electron Delocalization Another possible interpretation is the difference in the stabilization interaction of the pyrazole 2-nitrogen lone-pair electrons with the C=O σ* orbital in the *E*-conformation (Figure 7(b)) or with the C–C σ* orbital in the *Z*-conformation (Figure 7(c)) of *N*-acetyl pyrazole **2**. However, the former interaction is approximately null (IBE = –0.001 au), and the latter interaction is as small as –0.010 au (IBE). The interaction is insignificant. This is also likely because the distances of these orbitals are distal. Therefore, unexpectedly the N2 lone-pair electrons of the pyrazole and related heterocycles are not a determinant factor for the stereoselection of amides.

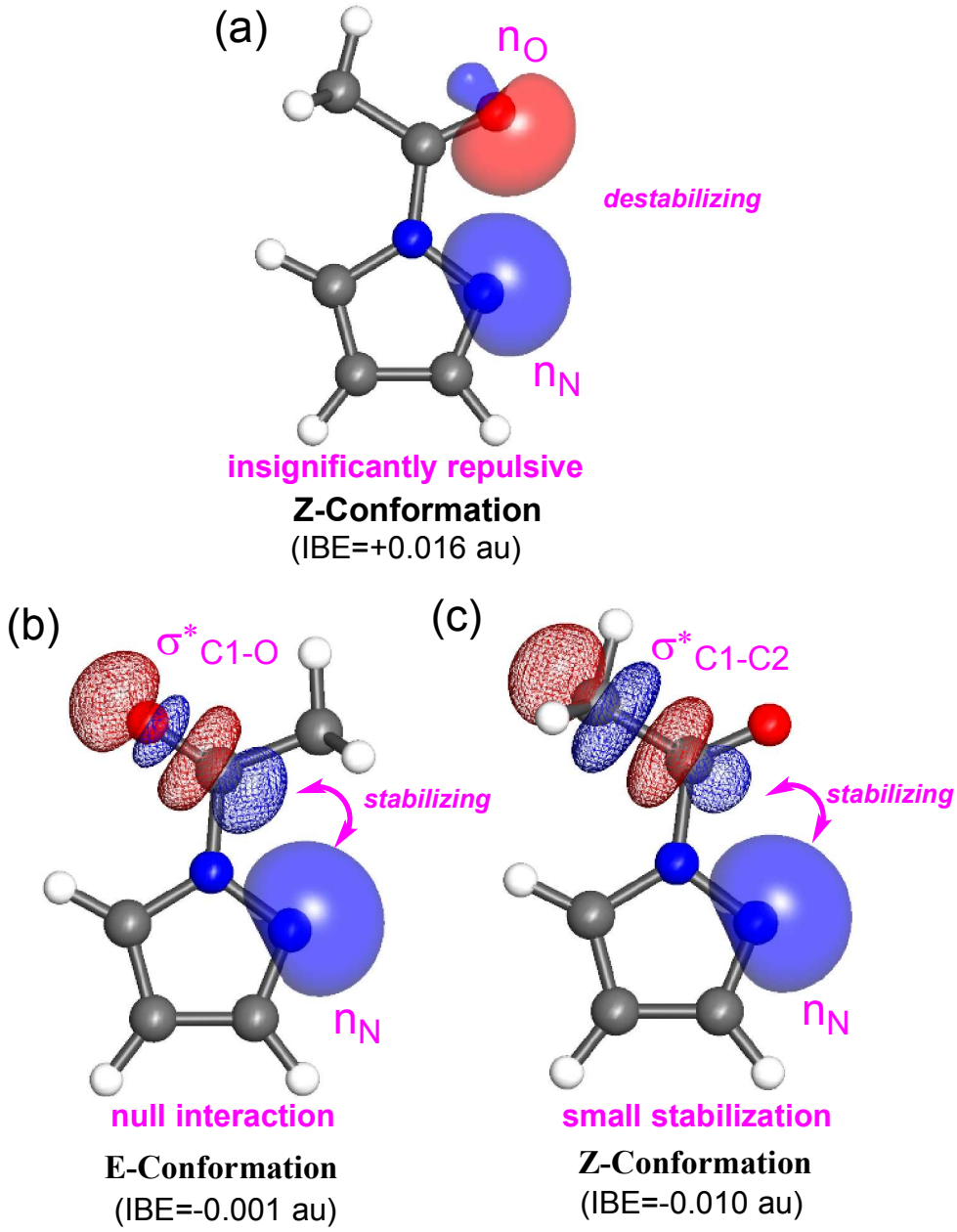

Figure 7. Three representative ineffective bond orbital interactions.

(a) repulsive interactions arising from lone-pair electrons of pyrazole 2-nitrogen (n_N) and the carbonyl oxygen atoms (n_O) in the *Z*-conformation. (b) delocalization interactions of the pyrazole 2-nitrogen lone-pair electrons into carbonyl σ*C1–O in the *E*-conformation (c) delocalization interactions of the pyrazole 2-nitrogen lone-pair electrons and into σ*C1–C2 in the *Z*-conformation. Isovalue 0.067 was used in all figures.

Conclusion

While most amides of the 1,3-diazole system (imidazoles) gave a mixture of *E* and *Z*, the overwhelming *E*-conformer preference at -90~100 °C was experimentally observed in the cases of the 2-*N*-heterocyclic amides [*N*-acyl pyrazoles (**2**, **6**, **13**, and **14**), *N*-acyl-1, 2, 3-triazoles (**3** and **7**), and *N*-acyl-1, 2, 4-triazoles (**4** and **8**)]. The analysis of orbital interactions based on the IBE calculations suggested that the *Z*-conformer is involved in the strong vicinal σ-σ orbital repulsion arising from the C2–C1 <---> N1–N2 and C2–C1 <---> N1–C5 moieties along the amide linkage, which destabilizes the *Z*-conformer to a great extent, leading to the overwhelming *E*-conformer preference. Repulsive interaction between two sets of lone-pair electrons on the pyrazole 2-nitrogen (n_N) and the carbonyl oxygen atoms (n_O) in the *Z*-conformation of *N*-acyl pyrazole is insignificant. Thus, the energy difference in the repulsive interaction of n_O–n_N between the *Z*- and *E*-conformations of *N*-acyl pyrazole is much smaller than that of the above-mentioned σ–σ electron repulsion. The n-σ* of the pyrazole 2-nitrogen lone-pair electrons is also negligible. Therefore, the origin of the conformational preference is counter-intuitive. On the other hand, in the case of imidazole derivatives, these vicinal σ–σ repulsions with respect to the amide bond are counterbalanced (*N*-acetyl imidazole **1**, see the Supporting Information), leading to a weak preference for the *E*-conformer over the *Z*-conformer. Conventionally, *N*-acyl azoles have been used as mild acylating agents since they were considered to be unstable and highly reactive. In contrast, our study elucidated that *N*-2',4,6'-trisubstituted benzoyl pyrazoles/triazoles are stable and have the *E*-specific conformation at body temperature. These *N*-2',4,6'-trisubstituted benzoyl pyrazoles/triazoles are expected to be utilized as new basic scaffolds for the design of bioactive compounds in medicinal chemistry in future.

Experimental

General experimental methods and instrumentation.

Materials were obtained from commercial suppliers. NMR spectra were recorded on a spectrometer at 600 MHz for ^{1}H-NMR, and 150 MHz for ^{13}C-NMR. Chemical shifts are given in parts per million (ppm) downfield from tetramethylsilane as an internal standard, and coupling constants (*J*) are reported in Hertz (Hz). Splitting patterns are abbreviated as follows: singlet (s), doublet (d), triplet (t), quartet (q), multiplet (m), and broad singlet (bs). IR spectra were recorded on a FT-IR spectrometer equipped with ATR (Diamond). The high-resolution mass spectra (HRMS) were obtained with an ionization mode of ESI/TOF. Melting points were recorded on a melting point apparatus and are uncorrected. Optical rotations were determined with a digital polarimeter. Analytical thin-layer chromatography was performed on precoated, glass-backed silica gel plates. Column chromatography was performed using silica gel (45–60 μm). Extracted solutions were dried over anhydrous $MgSO_4$ or Na_2SO_4. Solvents were evaporated under reduced pressure.

Materials.

Spectral data for compounds **1**[6a,b], **2**[6a,b], **3**[6a], **4**[6a], **5a**[3], **5c**[3], **6a**[9], **7a**[10] are consistent with values previously reported in the literature.

General Experimental procedure for the syntheses of compounds 5-14.

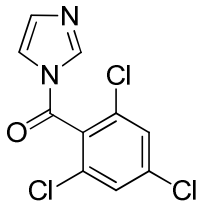

5b

To a solution of imidazole (68.1 mg, 1.0 mmol) in DMF (4 mL) was added successively NaH (90 mg in 60 % in oil, 1.5 mmol), and 2,4,6-trichlorobenzoyl chloride (365.9 mg, 1.5 mmol) at 0 °C. After being stirred at 23 °C for 2 hr, the reaction was quenched with ice-water and extracted with AcOEt. The organic layer was washed with sat. $NaHCO_3$, and dried over $MgSO_4$. After evaporation *in vacuo*, the residue was purified by silica gel column chromatography (AcOEt/hexane = 1:10) to give **5b** in 88% (242 mg, 0.88 mmol, *E*/*Z* = 2.5:1) as colorless crystals. mp 113 - 114 °C: ^{1}H NMR (600 MHz, $CDCl_3$, at 22 °C) δ 7.85 (bs, 1H, H2), 7.47 (s, 2H, H3', H5'), 7.39 (bs, 1H, H5), 7.15 (s, 1H, H4); ^{13}C NMR (150 MHz, $CDCl_3$) δ 160.6 (C=O), {138.3, 137.2, 133.3, 132.1, 131.0, 128.8, 128.0, 116.5} (Ar), IR (KBr) 1728 cm^{-1}; HRMS (ESI-TOF) *m/z*: $[M+H]^+$ Calcd for $C_{10}H_6N_2OCl_3$ 274.9540; Found 274.9543.

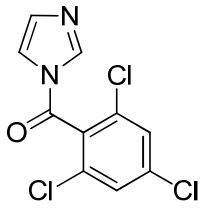

5b*E*

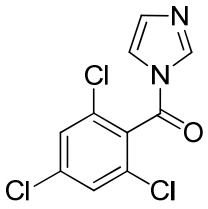

5b*Z*

Z-**5b**: ^{1}H NMR (600 MHz, CD_2Cl_2, at -90 °C) δ 8.48 (bs, 1H, H2), 7.45 (s, 2H, H3', H5'), 7.05 (s, 1H, H5), 6.81 (s, 1H, H4).

E-**5b**: ^{1}H NMR (600 MHz, CD_2Cl_2, at-90 °C) δ 7.76 (s, 1H, H2), 7.54 (s, 1H, H5), 7.50 (s, 2H, H3', H5'), 7.16 (s, 1H, H4).

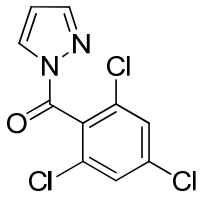

6b

Following the general procedure, compound **6b** was obtained after 2 h of reaction at 23 °C and was purified by silica gel column chromatography (AcOEt/hexane = 1:10), as powder in 92% yield (253.3 mg, 0.92 mmol): ^{1}H NMR (600 MHz, $CDCl_3$) δ 8.40 (bs, 1H, H5), 7.76 (s, 1H, H3), 7.72 (s, 2H, H3' ,H5'), 6.57 (s,1H, H4); ^{13}C NMR (150 MHz, $CDCl_3$) δ 162.8 (C=O), {145.9, 137.0, 133.1 , 132.4, 128.9, 128.2, 111.2 } (Ar), IR (KBr) 1720 cm^{-1}; HRMS (ESI-TOF) *m/z*: $[M+Na]^+$ Calcd for $C_{10}H_5N_2OCl_3Na$ 296.9360; Found 296.9348.

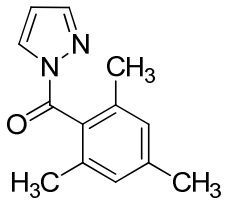

6c

Following the general procedure, compound **6c** was obtained after 2 h of reaction at 23 °C and was purified by silica gel column chromatography (AcOEt/hexane = 1:4), as colorless crystals in 74% yield (126.0 mg, 0.59 mmol). mp 81 - 82 °C: ^{1}H NMR (600 MHz, $CDCl_3$) δ 8.42 (1H, bs, H5), 7.72 (1H, s, H3), 6.91 (s, 2H, H3', H5'), 6.50 (s, 1H, H4), 2.31(s, 3H, 4'-CH_3) , 2.14(s, 6H, 2',6'-CH_3); ^{13}C NMR (150 MHz, $CDCl_3$) δ 169.7 (C=O), {145.4, 140.1, 134.9, 131.4, 128.6, 128.4, 110.2} (Ar), 21.43, 19.34 (CH_3), IR (KBr) 1713 cm^{-1}; HRMS (ESI-TOF) *m/z*; $[M+Na]^+$ Calcd for $C_{13}H_{14}N_2ONa$ 237.0998; Found 237.0995.

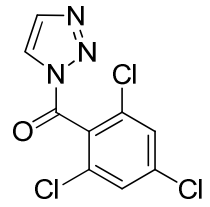

7b

Following the general procedure, compound **7b** was obtained after 2 h of reaction at 23 °C and was purified by silica gel column chromatography (AcOEt/hexane = 1:10), as powder in 71% yield (196 mg, 0.71 mmol): ^{1}H NMR (600 MHz, $CDCl_3$) δ 8.45 (s, 1H, H5), 7.85 (s, 1H, H4), 7.46 (s, 2H, H3' ,H5'); ^{13}C NMR (150 MHz, $CDCl_3$) δ 161.6 (C=O), {138.1, 135.0, 133.4, 131.0, 128.5, 121.9} (Ar), IR (KBr) 1743 cm^{-1}; HRMS (ESI-TOF) *m/z*: $[M+H]^+$ Calcd for $C_9H_5N_3OCl_3$ 275.9493; Found 275.9477.

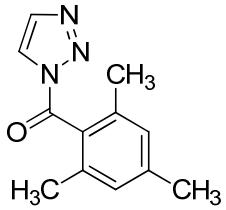

7c

Following the general procedure, compound **7c** was obtained after 2 h of reaction at 23 °C and was purified by silica gel column chromatography (AcOEt/hexane = 1:5), as colorless crystals in 69% yield (119 mg, 0.55 mmol). mp 85 - 86 °C: ^{1}H NMR (600 MHz, $CDCl_3$) δ 8.41 (s, 1H, H5), 7.80 (s, 1H, H4), 6.91 (s, 2H, H3', H5'), 2.31 (s, 3H, 4'-CH_3) , 2.14 (s, 6H, 2',6'-CH_3); ^{13}C NMR (150 MHz, $CDCl_3$) δ 168.2 (C=O), {141.2, 135.5, 134.5, 131.4, 130.0, 128.6, 122.0 } (Ar), 21.45,19.52 (CH_3), IR (KBr) 1743 cm^{-1}; HRMS (ESI-TOF) *m/z*: $[M+Na]^+$ Calcd for $C_{12}H_{13}N_3ONa$ 238.0951; Found 238.0965.

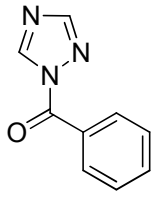

8a

To a solution of 1*H*-1,2,4-triazole (69.1 mg, 1.0 mmol) in DMF (4 mL) at 0 °C was added benzoyl chloride (70.3 mg, 0.5 mmol). After being stirred at 23 °C for 2 hr, the reaction was quenched with ice-water and extracted with AcOEt. The organic layer was dried over $MgSO_4$. After evaporation *in vacuo* to give **8a** in quantum yield (87 mg, 0.50 mmol) as powder: ^{1}H NMR (600 MHz, $CDCl_3$) δ 9.07 (s, 1H, H5), 8.04 (d, *J*= 7.8 Hz, 2H, H2', H6'), 8.10 (s, 1H, H3), 7.66 (t, *J*= 7.8 Hz,1H, H4'), 7.53 (t, *J*= 7.8 Hz, 2H, H3', H5'); ^{13}C NMR (150 MHz, $CDCl_3$) δ 164.7 (C=O), {153.5, 146.0, 135.4 , 134.4, 131.8, 131.5, 129.0, 128.4} (Ar), IR (KBr) 1713 cm^{-1}; HRMS (ESI-TOF) *m/z*: $[M+H]^+$ Calcd for $C_9H_8N_3O$ 174.0662; Found 174.0690.

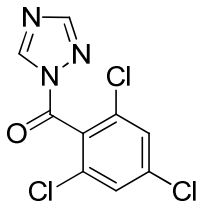

8b

Following the general procedure, compound **8b** was obtained after 2 h of reaction at 23 °C and was purified by silica gel column chromatography (AcOEt/hexane = 1:4), as colorless crystals in 79% yield (218 mg, 0.79 mmol). mp 105 - 106 °C: ^{1}H NMR (600 MHz, $CDCl_3$) δ 9.06 (s, 1H, H5), 8.04 (s, 1H, H3), 7.46 (s, 2H, H3', H5'); ^{13}C NMR (150 MHz, $CDCl_3$) δ 161.3 (C=O), {154.3, 144.3, 138.0, 133.1, 130.8, 128.4} (Ar), IR (KBr) 1743 cm^{-1}; HRMS (ESI-TOF) *m/z*: $[M+H]^+$ Calcd for $C_9H_5N_3OCl_3$ 275.9493; Found 275.9491.

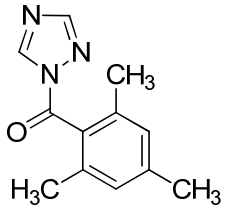

8c

Following the general procedure, compound **8c** was obtained after 2 h of reaction at 23 °C and was purified by silica gel column chromatography (AcOEt/hexane = 1:4), as colorless crystals in 60% yield (104 mg, 0.48 mmol). mp 88 - 90 °C: ^{1}H NMR (600 MHz, $CDCl_3$, at 22 °C) δ 8.94 (bs, 1H, H5), 8.04 (s, 1H, H3), 6.95 (s, 2H, H3', H5'), 2.31 (s, 3H, 4'-CH_3) , 2.17 (s, 6H, 2',6'-CH_3); ^{13}C NMR (150 MHz, $CDCl_3$) δ 167.7 (C=O), {154.1, 144.5, 141.1, 135.1, 129.8, 128.7}(Ar), 21.45, 19.42 (CH_3), IR (KBr) 1728 cm^{-1}; HRMS (ESI-TOF) *m/z*: $[M+Na]^+$ Calcd for $C_{12}H_{13}N_3ONa$ 238.0951; Found 238.0949.

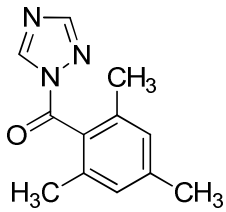

8c*E*

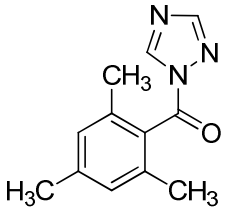

8c*Z*

Z-**8c**: ^{1}H NMR (600 MHz, CD_2Cl_2, at -90 °C) δ 8.16 (s, 1H, H5), 8.10 (s, 1H, H3), 6.93 (s, 2H, H3', H5'), 2.31 (s, 3H, 4'-CH_3), 2.12 (s, 6H, 2',6'-CH_3)

E-**8c**: ^{1}H NMR (600 MHz, CD_2Cl_2, at -90 °C) δ 9.09 (s, 1H, H5), 7.94 (s, 1H, H3), 6.88 (s, 2H, H3', H5'), 2.27 (s, 3H, 4'-CH_3), 2.08 (s, 6H, 2',6'-CH_3)

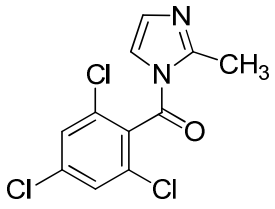

9b

Following the general procedure, compound **9b** was obtained after 2 h of reaction at 23 °C and was purified by silica gel column chromatography (AcOEt/hexane = 1:4), as colorless crystals in 73% yield (212 mg, 0.73 mmol). mp 122-123 °C: ^{1}H NMR (600 MHz, $CDCl_3$, at 22 °C) δ 7.47 (s, 2H, H3', H5'), 6.93 (bs, 1H, H5), 6.77 (s, 1H, H4) 2.77(s, 3H, CH_3); ^{13}C NMR (150 MHz, $CDCl_3$ at 22 °C) δ 161.7 (C=O), {138.2, 132.9, 131.7, 128.8, 127.8, 118.2} (Ar), 16.67(CH_3), IR (ATR) 1718 cm^{-1}; HRMS (ESI-TOF) *m/z*: $[M+H]^+$ Calcd for $C_{11}H_8N_2OCl_3$ 288.9697; Found 288.9698.

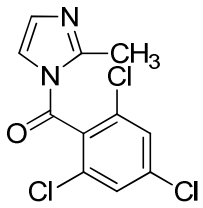

9b*E*

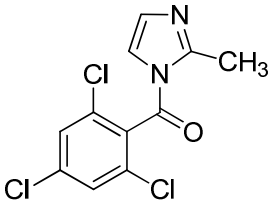

9b*Z*

Z-**9b**: ^{1}H NMR (600 MHz, CD_2Cl_2, at -90 °C) δ 7.45 (s, 2H, H3', H5'), 6.80 (s, 1H, H5), 6.67 (s, 1H, H4) 2.68 (s, 3H, CH_3)

E-**9b**: ^{1}H NMR (600 MHz, CD_2Cl_2, at -90 °C) δ 7.68 (s, 1H, H5), 7.48 (s, 2H, H3', H5'), 6.91 (s, 1H, H4) 2.68 (s, 3H, CH_3)

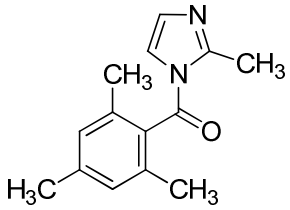

9c

Following the general procedure, compound **9c** was obtained after 2 h of reaction at 23 °C and was purified by silica gel column chromatography (AcOEt/hexane = 1:10), as powder in 63% yield (143 mg, 0.63 mmol): ^{1}H NMR (600 MHz, $CDCl_3$, at 22 °C) δ 6.92 (s, 2H, H3', H5'), 6.82 (s, 1H, H5), 6.75 (bs, 1H, H4), 2.69 (s, 3H, CH_3), 2.33 (s, 3H, 4'-CH_3), 2.16 (s, 6H, 2',6'-CH_3); ^{13}C NMR (150 MHz, $CDCl_3$) δ 169.2 (C=O), {148.0, 140.5, 134.5, 131.9, 128.8, 128.2, 118.8} (Ar), 21.35, 19.18, 17.28 (CH_3), IR (ATR) 1711 cm^{-1}; HRMS (ESI-TOF) *m/z*: $[M+H]^+$ Calcd for $C_{14}H_{17}N_2O$ 229.1335; Found 229.1328.

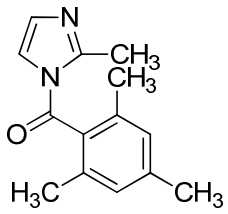

9c*E*

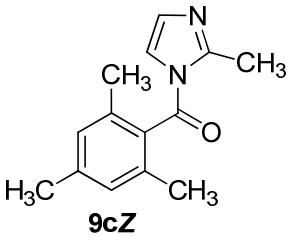

9c*Z*

Z-**9c**: ^{1}H NMR (600 MHz, CD_2Cl_2, at -90 °C) δ 6.89 (s, 2H, H3', H5'), 6.70 (s, 1H, H5), 6.59 (s, 1H, H4), 2.68 (s, 3H, 4'-CH_3), 2.24 (s, 3H, CH_3), 2.05 (s, 6H, 2',6'-CH_3)

E-**9c**: ^{1}H NMR (600 MHz, CD_2Cl_2, at -90 °C) δ 7.66 (s, 1H, H5), 6.90 (s, 2H, H3', H5'), 6.89 (s, 1H, H4), 2.68 (s, 3H, 4'-CH_3), 2.24 (s, 3H, CH_3), 2.05 (s, 6H, 2',6'-CH_3)

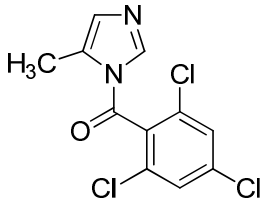

10b

Following the general procedure, compound **10b** was obtained after 2 h of reaction at 23 °C and was purified by silica gel column chromatography (AcOEt/hexane = 1:10), as powder in 14% yield (40 mg, 0.14 mmol): ^{1}H NMR (600 MHz, $CDCl_3$) δ 7.47 (s, 2H, H3', H5'), 7.38 (bs, 1H, H2), 6.86 (bs, 1H, H4), 2.58 (bs, 3H, CH_3); ^{13}C NMR (150 MHz, $CDCl_3$) δ 161.9 (C=O), {138.2, 137.9, 133.1, 131.9, 130.6, 128.7} (Ar), 12.06 (CH_3), IR (ATR) 1713 cm^{-1}; HRMS (ESI-TOF) *m/z*: $[M+H]^+$ Calcd for $C_{11}H_8N_2OCl_3$ 288.9697; Found 288.9698

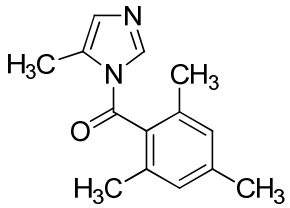

10c

Following the general procedure, compound **10c** was obtained after 2 h of reaction at 23 °C and was purified by silica gel column chromatography (AcOEt/hexane = 1:10), as powder in 19% yield (44 mg, 0.19 mmol): ^{1}H NMR (600 MHz, $CDCl_3$) δ 7.38 (bs, 1H, H2), 6.93 (s, 2H, H3', H5'), 6.82 (s, 1H, H4), 2.49 (bs, 3H, CH_3), 2.33 (s, 3H, 4'-CH_3), 2.17 (s, 6H, 2',6'-CH_3); ^{13}C NMR (150 MHz, $CDCl_3$) ^{13}C NMR (150 MHz, $CDCl_3$) δ 169.5 (C=O), {147.7, 139.0, 134.8, 131.7, 130.2, 128.8, 128.8} (Ar), 21.38, 19.25, 12.20 (CH_3), IR (ATR) 1721 cm^{-1}; HRMS (ESI-TOF) *m/z*: $[M+H]^+$ Calcd for $C_{14}H_{17}N_2O$ 229.1335; Found 229.1332.

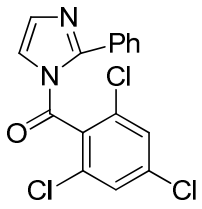

11b

Following the general procedure, compound **11b** was obtained after 2 h of reaction at 23 °C and was purified by silica gel column chromatography (AcOEt/hexane = 1:4), as a colorless crystals in 61% yield (216 mg, 0.61 mmol). mp 118 - 119 °C: ^{1}H NMR (600 MHz, $CDCl_3$, at 22 °C) δ 7.48 - 7.18 (m, 9H); ^{13}C NMR (150 MHz, $CDCl_3$) δ 161.6 (C=O), {149.2, 137.5, 133.4, 131.8, 130.3, 129.7, 129.1, 127.9, 118.8} (Ar), IR (ATR) 1714 cm^{-1}; HRMS (ESI-TOF) *m/z*: $[M+H]^+$ Calcd for $C_{16}H_{10}N_2OCl_3$ 350.9854; Found 350.9853.

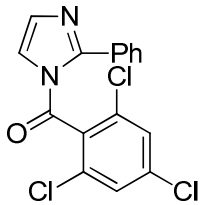

11b*E*

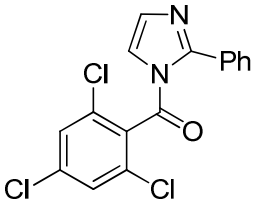

11b*Z*

Z-**11b**: ^{1}H NMR (600 MHz, CD_2Cl_2, at -90 °C) δ 7.63 - 7.61 (m, 2H, Ph), 7.48 (s, 2H, H3', H5'), 7.40 - 7.41 (m, 2H, Ph), 7.05 (m, 1H, Ph) 6.96 (s, 1H, H5), 6.85 (s, 1H, H4)

E-**11b**: ^{1}H NMR (600 MHz, CD_2Cl_2, at -90 °C) δ 7.81 (bs, 1H, H5), 7.43 (s, 2H, H3', H5') 7.23 (d, *J*=7.8 Hz, 2H, Ph), 7.20 (dd, *J*=6.6, 7.8Hz, 1H, Ph), 7.15 (bs, 1H, H4), 7.08 (dd, *J*=6.6, 7.8Hz, 2H, Ph).

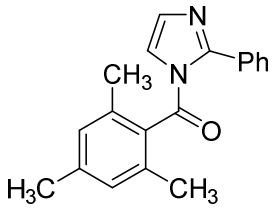

11c

Following the general procedure, compound **11c** was obtained after 2 h of reaction at 23 °C and was purified by silica gel column chromatography (AcOEt/hexane = 1:4), as a colorless crystals in 62% yield (170 mg, 0.62 mmol). mp 92 - 93 °C: ^{1}H NMR (600 MHz, $CDCl_3$) δ 7.58 - 7.57 (m, 2H, Ph), 7.37 - 7.35 (m, 3H, Ph), 7.06 (m, 1H, H5), 7.03 (bs, 1H, H4), 6.83 (s, 2H, H3', H5') , 2.27 (s, 3H, 4'-CH_3), 2.20 (s, 6H, 2',6'-CH_3); ^{13}C NMR (150 MHz, $CDCl_3$) δ 168.4 (C=O), {149.4, 140.7, 135.2, 131.3, 129.7, 129.3, 129.2, 128.9, 127.9, 119.9} (Ar), 21.28, 19.50 (CH_3), IR (ATR) 1732 cm^{-1}; HRMS (ESI-TOF) *m/z*: $[M+H]^+$ Calcd for $C_{19}H_{19}N_2O$ 291.1492; Found 291.1489.

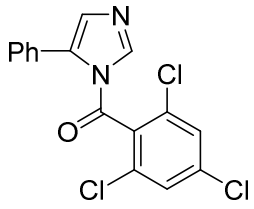

12b

To a solution of 1*H*-4- phenylimidazole (288.4 mg, 2 mmol) in DMF (4 mL) at 0 °C was added successively 2,4,6-trichlorobenzoyl chloride (243.9 mg, 1 mmol). After being stirred at 23 °C for 2 hr, the reaction was quenched with ice-water and extracted with AcOEt. The organic layer was washed with sat. $NaHCO_3$, and dried over $MgSO_4$. After evaporation *in vacuo*, the residue was purified by silica gel column chromatography (AcOEt/hexane = 1/4) to give **12b** in 2% yield (8 mg, 0.02 mmol) as colorless crystals. mp 95 - 96 °C: ^{1}H NMR (600 MHz, $CDCl_3$, at 22 °C) δ 8.10 (bs, 1H, H2), 7.32 - 7.23 (m, 7H), 7.09 (s, 1H, H4); ^{13}C NMR (150 MHz, $CDCl_3$) δ 161.4 (C=O), {138.7, 137.9, 133.5, 131.6, 131.4, 129.4, 128.9, 128.5, 128.4, 128.1} (Ar), IR (ATR) 1740 cm^{-1}; HRMS (ESI-TOF) *m/z*: $[M+H]^+$ Calcd for $C_{16}H_{10}N_2OCl_3$ 350.9853; found 350.9851.

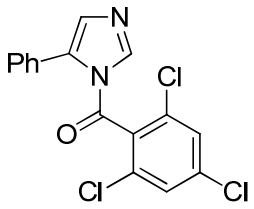

12b*E*

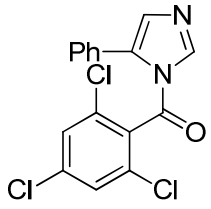

12b*Z*

Z-**12b**: ^{1}H NMR (600 MHz, CD_2Cl_2, at -90 °C) δ 8.42 (s, 1H, H2), 7.35 - 7.40 (m, 4H, H3', H5', Ph), 7.03 - 7.10 (m, 3H, Ph), 6.92 (s, 1H, H4)

E-**12b**: ^{1}H NMR (600 MHz, CD_2Cl_2, at -90 °C) δ 7.50 (s, 2H, H3', H5'), 7.35 - 7.40 (m, 4H, H2, Ph), 7.03 - 7.10 (m, 2H, H4, Ph), 6.94 (s, 1H, H4)

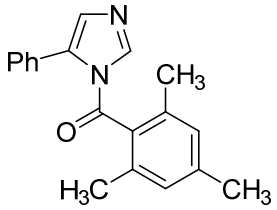

12c

To a solution of 1*H*-4- phenylimidazole (288.4 mg, 2 mmol) in DMF (4 mL) at 0 °C was added successively 2,4,6-trimethylbenzoyl chloride (182.7 mg, 1 mmol). After being stirred at 23 °C for 2 hr, the reaction was quenched with ice-water and extracted with AcOEt. The organic layer was washed with sat. $NaHCO_3$, and dried over $MgSO_4$. After evaporation *in vacuo*, the residue was purified by silica gel column chromatography (AcOEt/hexane = 1/4) to give **12c** (8 mg, 0.03 mmol, 3%) as colorless crystals. mp 90 - 92 °C: ^{1}H NMR (600 MHz, $CDCl_3$) δ 7.63 (bs, 1H, H2), 7.35 - 7.42 (m, 5H, Ph), 6.87 (s, 1H, H4), 6.87 (s, 2H, H3',H5'), 2.30 (s, 3H, 4'-CH_3), 2.22

(s, 6H, 2',6'-CH_3); ^{13}C NMR (150 MHz, $CDCl_3$) δ 168.1 (C=O), {141.0, 139.9, 135.4, 133.0, 131. 9, 131.2, 129.1, 128.9, 128.4, 128.1} (Ar), 21.32, 19.52 (CH_3), IR (ATR) 1727 cm^{-1}; HRMS (ESI-TOF) *m/z*: $[M+H]^+$ Calcd for $C_{19}H_{19}N_2O$ 291.1492; Found 291.1489.

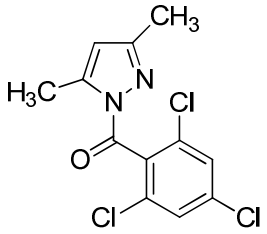

13b

Following the general procedure, compound **13b** was obtained after 2 h of reaction at 23 °C and was purified by silica gel column chromatography (AcOEt/hexane = 1:10), as a colorless crystals in 69% yield (210 mg, 0.69 mmol). mp 117-118 °C: ^{1}H NMR (600 MHz, $CDCl_3$) δ 7.37 (s, 2H, H3', H5'), 6.05 (s, 1H, H4) , 2.67 (s, 3H, CH_3), 2.16 (s, 3H, CH_3); ^{13}C NMR (150 MHz, $CDCl_3$) δ 164.2 (C=O), {154.3, 144.4, 136.0, 134.3, 132.7, 128.0} (Ar) 14.19, 14.06(CH_3), IR (ATR) 1718 cm^{-1}; HRMS (ESI-TOF) *m/z*: $[M+H]^+$ Calcd for $C_{12}H_{10}N_2OCl_3$ 302.9853; Found 302.9848.

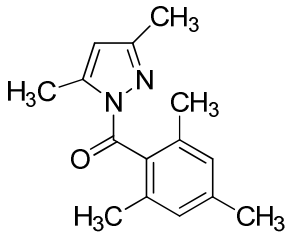

13c

Following the general procedure, compound **13c** was obtained after 2 h of reaction at 23 °C and was purified by silica gel column chromatography (AcOEt/hexane = 1:10), as a colorless crystals in 86% yield (208 mg, 0.86 mmol). mp 60-61 °C: ^{1}H NMR (600 MHz, $CDCl_3$) δ 6.88 (s, 2H, H3' ,H5'), 6.01 (s, 1H, H4), 2.64 (bs, 3H, CH_3), 2.31 (s, 3H, 4'-CH_3), 2.15 (s, 3H, CH_3), 2.14 (s, 6H, 2',6'-CH_3); ^{13}C NMR (150 MHz, $CDCl_3$) δ 171.3 (C=O), {153.2, 144.0, 139.2, 134.5, 133.6, 128.7, 111.6} (Ar), 21.42, 19.45, 14.57, 14.09 (CH_3), IR (ATR) 1728 cm^{-1}; HRMS (ESI-TOF) *m/z*: $[M+H]^+$ Calcd for $C_{15}H_{19}N_2O$ 243.1492; Found 243.1487.

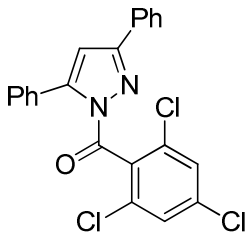

14b

Following the general procedure, compound **14b** was obtained after 2 h of reaction at 23 °C and was purified by silica gel column chromatography (AcOEt/hexane = 1:10), as a colorless crystals

in 19% yield (82 mg, 0.19 mmol). mp 154 – 155 °C: ^{1}H NMR (600 MHz, $CDCl_3$) δ 7.73 (bs, 2H, 5-Ph), 7.61 (bs, 2H, 3-Ph) 7.25 – 7.46 (m, 8H), 6.83 (s, 1H, H4); ^{13}C NMR (150 MHz, $CDCl_3$) δ 163.4 (C=O), {155.2, 147.7, 136.1, 134.1, 130.0, 129.6, 128.9, 128.5, 128.3, 128.0, 126.6, 110.9 }(Ar) , IR (ATR) 1738 cm^{-1}; HRMS (ESI-TOF) *m/z*: $[M+H]^+$ Calcd for $C_{22}H_{14}N_2OCl_3$ 427.0166; Found 427.0174.

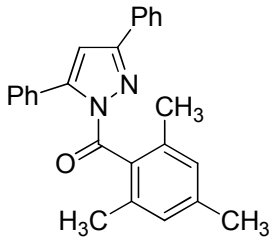

14c

Following the general procedure, compound **14c** was obtained after 2 h of reaction at 23 °C and was purified by silica gel column chromatography (AcOEt/hexane = 1:10), as oil in 27% yield (100 mg, 0.27 mmol): ^{1}H NMR (600 MHz, $CDCl_3$) δ 7.74 – 7.76 (m, 2H, 5-Ph), 7.55 – 7.56 (m, 2H, 3-Ph), 7.43 – 7.46 (m, 3H, 5-Ph), 7.35 – 7.39 (m, 3H, 2-Ph), 6.88 (s, 2H, H3', H5'), 6.80 (s, 1H, H4), 2.33 (s, 3H, 4'-CH_3), 2.24 (s, 6H, 2',6'-CH_3); ^{13}C NMR (150 MHz, $CDCl_3$) δ 170.3 (C=O), {154.3, 147.5, 135.2, 133.0, 131.9, 131.0, 129.2, 129.1, 129.0, 128.8, 128.3, 128.2, 126.5, 110.1} (Ar), 21.40, 19.82 (CH_3), IR (ATR) 1739 cm^{-1}; HRMS (ESI-TOF) *m/z*: $[M+H]^+$ Calcd for $C_{25}H_{23}N_2O$ 367.1805; Found 367.1805.

Line Shape Analysis

Line shape analysis was carried out with a program, DNMR (Bruker Biospin). Line shape analysis was performed by iterative matching of the simulated spectra with the experimental spectra. Rate constants were obtained at several temperatures, then activation parameters, free energies of activation ($\Delta G^{\ddagger}$), enthalpies ($\Delta H^{\ddagger}$) and activation entropies ($\Delta S^{\ddagger}$) and errors for the process of line shape matching were obtained by least-squares analysis of the Eyring plots:

$$\ln\frac{k}{T} = -\frac{\Delta H^{\ddagger}}{RT} + \frac{\Delta S^{\ddagger}}{R} + \ln\frac{k_B}{h}$$

$$\Delta \boldsymbol{G}^{\ddagger} = \Delta \boldsymbol{H}^{\ddagger} - \mathbf{T}\Delta \boldsymbol{S}^{\ddagger}$$

We showed the free energies of activation ($\Delta G^{\ddagger}$) at the coalescence temperature for the isomerization from *E* form to *Z* form. The detail of the data was shown in Supporting Information.

Supporting Information

The supporting information is available free of charge on the ACS Publications website

Stability studies of *N*-2'4'6'-trichlorobenzoylazoles (**5b**, **6b**, **7b**, **8b**)

Stereochemical stability of the *E*/*Z* diastereomers of compounds (**1**, **5b**, **5c**, **8c**, **9b**, **9c**, **11b**, **12b**)

X-ray structure analysis of compounds **6b, 7b, 8b, 9b, 11b, 13b, 14b.**

Computational studies

^{1}H-, ^{13}C-, HH-COSY-, and CH-COSY-NMR Spectra

Acknowledgments

This work was supported in part by a Grant-in-Aid for Scientific Research (C) (15K08030) from the Japan Society for the Promotion of Science. H.T. thanks the MEXT-Supported Program for the Strategic Research Foundation at Private Universities (2013-2017), and Hoansha Foundation for financial support. The computations were performed at the Research Center for Computational Science, Okazaki, Japan. We thank the computational facility for generous allotments of computer time.

REFERENCES AND NOTES

(1) (a) Staab, H. A. *Angew. Chem. Int. Ed.* **1962**, *1*, 351–367. (b) Jursic, B. S.; Zdravkovski, Z. *J. Mol. Struct.* **1994**, *303*, 177–183.

(2) (a) Kise, N.; Morimoto, S. *Tetrahedron* **2008**, *64*, 1765–1771. (b) Lu, Y.; Wei, P.; Pei, Y.; Xu, H.; Xin, X.; Pei, Z. *Green Chemistry* **2014**, *16*, 4510–4514.

(3) (a) Staab, H. A. *Chem. Ber.* **1956**, *89*, 2088–2093. (b) Zaramella, S.; Strömberg, R.; Yeheskiely, E. *Eur. J. Org. Chem.* **2002**, 2633–2639.

(4) (a) Tabata, H.; Yoneda, T.; Oshitari, T.; Takahashi, H.; Natsugari, H. *J. Med. Chem.* **2017**, *60*, 4503–4509. (b) Yoneda, T.; Tabata, H.; Tasaka, T.; Oshitari, T.; Takahashi, H.; Natsugari, H. *J. Med. Chem.* **2015**, *58*, 3268–3273. (c) Tabata, H.; Kayama, S.; Takahashi, Y.; Tani, N.; Wakamatsu, S.; Tasaka, T.; Oshitari, T.; Natsugari, H.; Takahashi, H. *Org. Lett.* **2014**, *16*, 1514–1517. (d) Wakamatsu, S.; Takahashi, Y.; Tabata, H.; Oshitari, T.; Tani, N.; Azumaya, I.; Katsumoto, Y.; Tanaka, T.; Hosoi, S.; Natsugari, H.; Takahashi, H. *Chem.-Eur. J.* **2013**, *19*, 7056–7063. (e) Takahashi, H.; Wakamatsu, S.; Tabata, H.; Oshitari, T.; Harada, A.; Inoue, K.; Natsugari, H. *Org. Lett.* **2011**, *13*, 760–763. (f) Tabata, H; Nakagomi, J.; Morizono, D.; Oshitari, T.; Takahashi, H.; Natsugari, H. *Angew. Chem. Int. Ed.* **2011**, *50*, 3075–3079.

(5) Takahashi, Y.; Wakamatsu, S.; Tabata, H.; Oshitari, T.; Natsugari, H.; Takahashi, H. *Synthesis* **2015**, *47*, 2125–2128.

(6) (a) Pappalardo, L.; Elguero, J.; Marzin, C. *Compt. Rend., ser. C*. **1973**, *277*, 1163–1166. (b) Luboch, E.; Biernat, J. F. *Polish J. Chem.* **1982**, *56*, 1151–1156.

(7) For determination of $\Delta G^{\ddagger}$ value, see: (a) Clark, A. J.; Curran, D. P.; Fox, D. J.; Ghelfi, F; Guy, C. S.; Hay, B.; James, N.; Phillips, J. M.; Roncaglia, F.; Sellars, P. B.; Wilson, P. *J. Org. Chem.* **2016**, *81*, 5547-5565. (b) Lewis, A.; Rutherford, T. J.; Wilkie J.; Jenn, T.; Gani, D. *J. Chem. Soc., Perkin Trans 1*. **1998**, 3795–3806.

(8) A conversion factor of 1 cal = 4.184 J was used in all calculations.

(9) Tensmeyer, L. G.; Ainsworth, C. *J. Org. Chem.*, **1966**, *31,* 1878–1883.

(10) Holzer, W. *Tetrahedron*, **1991**, *47*, 9783–9792.

(11) It is debatable whether the conformation of **5a** which appeared in the VT-NMR spectrum is the average one between *E/Z*-amide conformers.

(12) The *Z*-conformation of compounds **5b**, **5c**, **8c**, **9b**, **9c**, and **11b** was assigned by cosnsidering the upfield shift of H5, which will stand in the shielding cone of the aryl group.

(13) The very small peaks were observed at –90 °C in **5c** and **8c**. Although it is difficult to explain the origin of these peaks, the partly reduced rotation of the C7'—C1' bond might be responsible.

(14) The regioisomers, 3-phenyl imidazole derivatives, were obtained as major compounds.

(15) (a) We obtained the electronic structures of molecules **2** and **6b** at the HF/6-31G(d) level using the optimized geometries at B3LYP/6-311G(d,p). The electronic structures were analyzed using the bond model analysis program. (b) The bond model analysis program is available on the website: http://orbitalphase.web.fc2.com/.

(16) Naruse, Y.; Ma, J.; Takeuchi, K.; Nohara, T.; Inagaki, S. *Tetrahedron* **2006**, *62*, 4491–4497 and references therein. See also: Inagaki, S., *Orbital in Chemistry* **2009**, Springer, Heidelberg.